Geophysical Prospecting, 2009, **57**, 13–26 doi: 10.1111/j.1365-2478.2008.00732.x

Migration velocity analysis for tilted transversely isotropic media

Laxmidhar Behera[1,2] and Ilya Tsvankin[2]*

[1]*National Geophysical Research Institute, Hyderabad 500007, India, and* [2]*Colorado School of Mines, Department of Geophysics, Center for Wave Phenomena, Golden, CO 80401-1887, USA*

Received July 2007, revision accepted April 2008

ABSTRACT

Tilted transversely isotropic formations cause serious imaging distortions in active tectonic areas (e.g., fold-and-thrust belts) and in subsalt exploration. Here, we introduce a methodology for P-wave prestack depth imaging in tilted transversely isotropic media that properly accounts for the tilt of the symmetry axis as well as for spatial velocity variations.

For purposes of migration velocity analysis, the model is divided into blocks with constant values of the anisotropy parameters ϵ and δ and linearly varying symmetry-direction velocity V_{P0} controlled by the vertical (k_z) and lateral (k_x) gradients. Since determination of tilt from P-wave data is generally unstable, the symmetry axis is kept orthogonal to the reflectors in all trial velocity models. It is also assumed that the velocity V_{P0} is either known at the top of each block or remains continuous in the vertical direction. The velocity analysis algorithm estimates the velocity gradients k_z and k_x and the anisotropy parameters ϵ and δ in the layer-stripping mode using a generalized version of the method introduced by Sarkar and Tsvankin for factorized transverse isotropy with a vertical symmetry axis.

Synthetic tests for several models typical in exploration (a syncline, uptilted shale layers near a salt dome and a bending shale layer) confirm that if the symmetry-axis direction is fixed and V_{P0} is known, the parameters k_z, k_x, ϵ and δ can be resolved from reflection data. It should be emphasized that estimation of ϵ in tilted transversely isotropic media requires using nonhyperbolic moveout for long offsets reaching at least twice the reflector depth. We also demonstrate that application of processing algorithms designed for a vertical symmetry axis to data from tilted transversely isotropic media may lead to significant misfocusing of reflectors and errors in parameter estimation, even when the tilt is moderate (30°). The ability of our velocity analysis algorithm to separate the anisotropy parameters from the velocity gradients can be also used in lithology discrimination and geologic interpretation of seismic data in complex areas.

INTRODUCTION

Transverse isotropy with a tilted symmetry axis (TTI) is a model often used to describe dipping shale layers in active tectonic areas such as the Canadian Foothills and near salt bodies (e.g., Vestrum, Lawton and Schmid 1999; Tsvankin 2005). TTI symmetry can also be created by systems of parallel dipping fractures embedded in otherwise isotropic rock (Angerer *et al.* 2002; Dewangan and Tsvankin 2006a,b). Serious distortions caused by TTI layers in conventional (isotropic) seismic imaging are well documented in the literature (e.g., Isaac and Lawton 1999; Vestrum *et al.* 1999). To properly image targets overlaid by TTI formations, migration algorithms have to be able to handle the tilt of the symmetry

*E-mail: ilya@mines.edu

axis, which often varies laterally (Kumar, Sen and Ferguson 2004). Since the influence of tilt creates ambiguity in parameter estimation, a major problem in seismic processing for TTI media is accurate velocity analysis and model building.

P-wave kinematic signatures for tilted transverse isotropy can be described by the symmetry-direction velocity V_{P0}, Thomsen (1986) parameters ϵ and δ and two angles responsible for the orientation of the symmetry axis. In 2D models treated here, the symmetry direction is described by the angle ν (tilt) with the vertical. Estimation of this set of parameters even for a single horizontal or dipping TTI layer generally requires combining P-wave data with mode-converted PS-waves (Dewangan and Tsvankin 2006a,b). Inversion of P-wave reflection traveltimes alone for the TTI parameters is nonunique, unless NMO ellipses from reflectors with two different dips are available (Grechka and Tsvankin 2000).

For TTI shale layers, the symmetry axis is usually orthogonal to the layer boundaries, which helps to reduce the number of independent parameters and makes velocity analysis more stable. If the dip ϕ of the reflector is equal to the tilt ν, the dip-line P-wave normal-moveout (NMO) velocity in a homogeneous TTI layer is described by the isotropic cosine-of-dip dependence (Tsvankin 1995, 1997):

$$V_{\rm nmo}(\phi) = \frac{V_{\rm nmo}(0)}{\cos\phi} = \frac{V_{\rm nmo}(0)}{\sqrt{1 - p^2 V_{P0}^2}}, \qquad (1)$$

where $p = \sin\phi / V_{P0}$ is the ray parameter of the zero-offset ray; note that p can be determined from time slopes on the zero-offset or stacked section. In some cases (e.g., for a bending layer that has a horizontal segment), it may be possible to directly estimate the zero-dip NMO velocity given by:

$$V_{\rm nmo}(0) = V_{P0}\sqrt{1 + 2\delta}\,. \qquad (2)$$

Then equation (1) can be used to find the vertical velocity V_{P0}, which can be substituted into equation (2) to obtain δ. Still, the parameter ϵ even in this simple model remains unconstrained by the P-wave NMO velocity from the bottom of the layer. Grechka *et al.* (2001) demonstrate on physical-modeling data that for relatively simple models it may be possible to estimate ϵ in a TTI layer using the NMO velocities for reflections from deeper interfaces.

Additional information about the anisotropy parameters is provided by nonhyperbolic moveout. If the symmetry axis is orthogonal to the bottom of a TTI layer, the P-wave quartic moveout coefficient on the dip line of the reflector is proportional to the Alkhalifah-Tsvankin (1995) anellipticity parameter $\eta \equiv (\epsilon - \delta)/(1 + 2\delta)$ (Pech, Tsvankin and Grechka 2003). Therefore, if δ has been found by inverting NMO velocity, nonhyperbolic moveout can be used to constrain ϵ. These parameter-estimation issues have serious implications for migration velocity analysis (MVA) in TTI media discussed here.

An efficient MVA method for transversely isotropic media with a vertical symmetry axis (VTI) was introduced by Sarkar and Tsvankin (2004), who divided the model into factorized VTI blocks. A medium is called factorized if all ratios of the stiffness elements c_{ij} are constant, which implies that the anisotropy parameters are constant as well. In general, the reference velocity (in our case, V_{P0}) in factorized models represents an arbitrary function of the spatial coordinates (Červený 1989). Factorized transverse isotropy with a linear velocity function $V_{P0}(x, z)$ is the simplest 2D model that accounts for both anisotropy and heterogeneity:

$$V_{P0}(x, z) = V_{P0}(0, 0) + k_x x + k_z z; \qquad (3)$$

k_x and k_z are the horizontal and vertical velocity gradients.

Since anisotropy parameters are usually obtained with a relatively low spatial resolution, neglecting their variation within factorized blocks does not significantly impair the quality of the velocity model. Sarkar and Tsvankin (2003, 2004, 2006) demonstrate on synthetic and field data that if the velocity V_{P0} varies linearly and is known at a single point in each factorized VTI block, the MVA algorithm accurately estimates the parameters ϵ and δ along with the velocity gradients k_x and k_z. It should be emphasized that stable recovery of the parameter ϵ (or η) in VTI media requires using either long-spread data (with the maximum offset-to-depth ratio of at least two) or dipping events.

Here, we extend the MVA algorithm of Sarkar and Tsvankin (2004) to tilted transverse isotropy. The symmetry axis is confined to the vertical incidence plane and assumed to be orthogonal to the reflector beneath a TTI layer. The model is divided into TTI blocks with constant values of ϵ and δ and a linearly varying symmetry-direction velocity V_{P0} (equation (3)). These blocks, however, are not strictly factorized because the symmetry axis is kept orthogonal to reflectors, which may have arbitrary shape. As a result, the symmetry-axis direction and, therefore, the ratios of the stiffnesses c_{ij} may vary within each block. (Note that the stiffness ratios remain constant in the rotated coordinate system tied to the symmetry axis.)

We begin by introducing the methodology of Kirchhoff prestack depth migration and migration velocity analysis for TTI media. Then the method is tested on several typical TTI models that include dipping anisotropic layers. The velocity-analysis and imaging results are compared with those obtained by VTI algorithms to illustrate the need to account

for tilt in anisotropic imaging. We also study the influence of spreadlength on the errors in the medium parameters and show that the parameter ϵ cannot be constrained without evaluating residual moveout for large (reaching at least two) offset-to-depth ratios.

METHODOLOGY

The migration velocity analysis algorithm of Sarkar and Tsvankin (2004), designed for piecewise-factorized VTI media, includes the same two main steps as conventional MVA in isotropic media (e.g., Liu and Bleistein 1995). Kirchhoff depth migration with a trial velocity model creates an image of the subsurface. After picking reflectors on the migrated section, semblance scanning is used to evaluate the residual moveout of reflection events in image gathers (often called 'common image gathers' in the offset domain). The second step is a linearized parameter update (implemented following the algorithm discussed in Sarkar and Tsvankin 2004, Appendix A) designed to minimize the residual moveout after the next application of migration. The two steps are iterated until events in image gathers are sufficiently flat.

Sarkar and Tsvankin (2004) estimate the vertical velocity gradient k_z by using two reflectors located at different depths in each factorized block. To constrain the parameter η (and, therefore, ϵ), the residual moveout in image gathers is described by the following nonhyperbolic equation:

$$z_M^2(h) = z_M^2(0) + r_1 h^2 + r_2 \frac{h^4}{h^2 + z_M^2(0)}, \qquad (4)$$

where z_M is the migrated depth and h is the half-offset. The coefficients r_1 and r_2, which quantify the magnitude of residual moveout, are estimated by a 2D semblance scan. The goal of the iterative MVA algorithm is to flatten image gathers by minimizing r_1 and r_2. The coefficient r_2 is sensitive to the parameter η, which is primarily responsible for nonhyperbolic moveout at long offsets.

To make the modeling and migration algorithms of Sarkar and Tsvankin (2004) suitable for a medium composed of 'quasi-factorized' TTI blocks or layers, we use ray-tracing software that can handle an arbitrary tilt of the symmetry axis (Seismic Unix codes 'unif2aniso' and 'sukdsyn2d'; see Alkhalifah 1995). The model is assumed to be 2D, with the vertical incidence plane containing the symmetry axis and, therefore, the reflector normals. At the parameter-estimation step, we keep the symmetry axis orthogonal to the reflectors picked on the trial image and update the parameters ϵ and δ and the velocity gradients k_z and k_x(ϵ, δ, k_z and k_x are kept constant within each block). As in the VTI case, the velocity V_{P0} has to be known at one point in each factorized block; for example, it can be specified at the top of the model and assumed to be continuous in the vertical direction. The MVA is applied in the layer-stripping mode starting at the top of the model.

The matter of dividing the section into blocks is non-trivial and can influence both the parameter-estimation results and image quality. Stable inversion for the velocity gradients requires each block to include two well-separated reflecting interfaces with a sufficient lateral extent. In general, one should use the minimum number of blocks needed to remove the residual moveout in image gathers throughout the section. The case study of Sarkar and Tsvankin (2006) shows that even for a relatively complicated 2D section image gathers can be flattened using only 5-6 factorized blocks. In practice, we first perform parameter estimation for two shallow reflectors (e.g., on the left-hand side of the section) and then analyse image gathers for the obtained velocity model. The part of the section with flat image gathers is then designated as the first block and the parameters of this block are used to continue MVA for the rest of the section.

Note that for TTI media with a positive vertical gradient in V_{P0}, reflections from steeply dipping interfaces often arrive at the surface as *turning* rays (Tsvankin 1997, 2005). Hence, our algorithm is designed to properly account for turning-ray reflections in the computation of the traveltime field used by the migration operator.

TESTS ON SYNTHETIC DATA

Here, we generate synthetic seismograms and test our MVA/imaging algorithm on three common geologic models that often include tilted transversely isotropic formations: a syncline, a salt dome flanked by uptilted shale layers and a bending shale layer. To conform to our model assumptions, the symmetry axis is kept orthogonal to the bottom of the TTI layers.

Syncline model

The first model includes a TTI syncline with dips of 30° embedded in an otherwise isotropic section (Fig. 1). The isotropic layers are vertically heterogeneous but have no lateral velocity gradient, while the TTI layer is both vertically and laterally heterogeneous. As required by the MVA algorithm, each layer contains two reflecting interfaces, with every second reflector representing the boundary between layers. Synthetic data

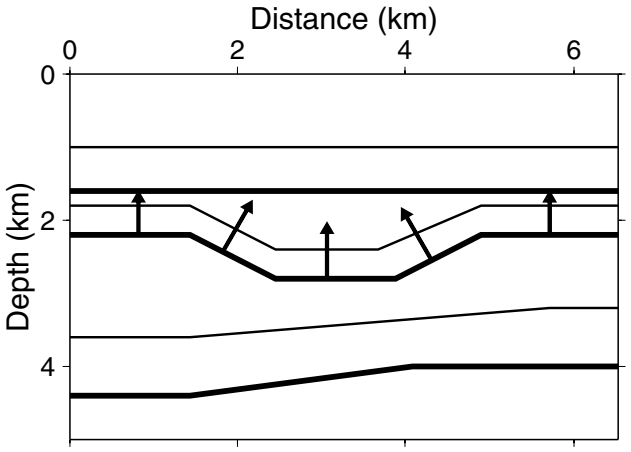

Figure 1 Model with a TTI syncline sandwiched between two isotropic layers. The bold lines mark the layer boundaries; the additional reflectors used in MVA are shown by the thinner lines. The parameters of the TTI layer are $V_{P0} = 2.3$ km/s, $k_z = 0.6\ s^{-1}$, $k_x = 0.1\ s^{-1}$, $\epsilon = 0.1$ and $\delta = -0.1$ ($\eta = 0.25$). The symmetry axis (marked by the arrows) is orthogonal to the layer's bottom; the dips are 30°. The top layer has $V_{P0} = 1.5$ km/s, $k_z = 1.0\ s^{-1}$ and $k_x = \epsilon = \delta = 0$; for the bottom layer, $V_{P0} = 2.7$ km/s, $k_z = 0.3\ s^{-1}$ and $k_x = \epsilon = \delta = 0$. The velocity V_{P0} is specified at the top of each layer at the 1 km coordinate.

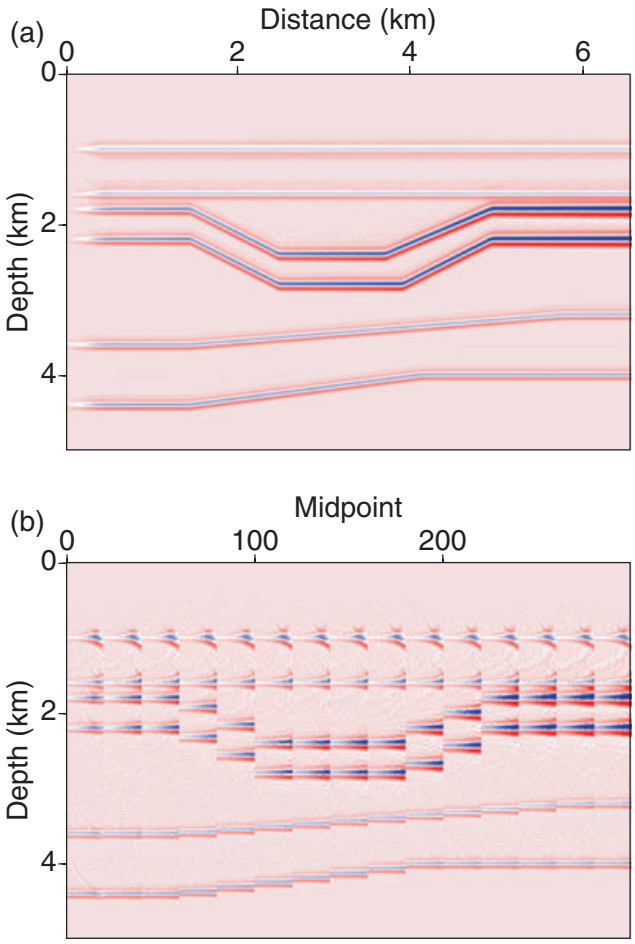

Figure 2 (a) True image of the model from Fig. 1 obtained by anisotropic prestack depth migration with the correct medium parameters. (b) The corresponding image gathers in the offset domain at 0.4 km intervals (displayed with the corresponding midpoints along the x-axis) for each reflector.

generated by anisotropic ray tracing consist of 260 shot gathers with shot and receiver intervals of 25 m.

The section obtained after anisotropic prestack depth-migration with the true model parameters for all layers is shown in Fig. 2(a). The influence of the tilt of the symmetry axis in the TTI layer is taken into account during the computation of the traveltime table by anisotropic ray tracing. Then the same traveltime table is used for Kirchhoff prestack depth-migration. As expected, all reflectors are well focused and accurately positioned and image gathers in Fig. 2(b) are perfectly flat.

TTI velocity analysis and migration

We applied our MVA algorithm to 10 image gathers located at horizontal coordinates ranging from 1.5 km to 5 km (Fig. 3). Since it is essential to use nonhyperbolic moveout in estimating the parameter ϵ in TTI media, the maximum offset-to-depth ratio for the bottom of the TTI layer is close to two. The medium parameters are obtained in the layer-stripping mode starting at the surface.

The initial velocity model used in the first iteration of MVA is homogeneous and isotropic. For the first (top) layer, the velocity V_{P0} is assumed to be known at a single surface location ($V_{P0}(x = 1\text{ km}, z = 0) = 1500$ m/s). This assumption, however, is needed only if this layer is treated as anisotropic. We also assign the correct value to the symmetry-direction velocity V_{P0} at the top of the second and third layers. The symmetry axis in the second layer is kept orthogonal to the layer's bottom.

The inverted parameters are close to the true values in all three layers and the migrated image (Fig. 3a) is practically indistinguishable from the benchmark section in Fig. 2(a). According to the analysis in the introduction, the NMO velocities from the horizontal and dipping reflectors in the TTI layer constrain the parameters V_{P0} and δ (see equations (1) and (2)). Although this result is obtained for a homogeneous TTI medium, it is likely to remain valid for our heterogeneous

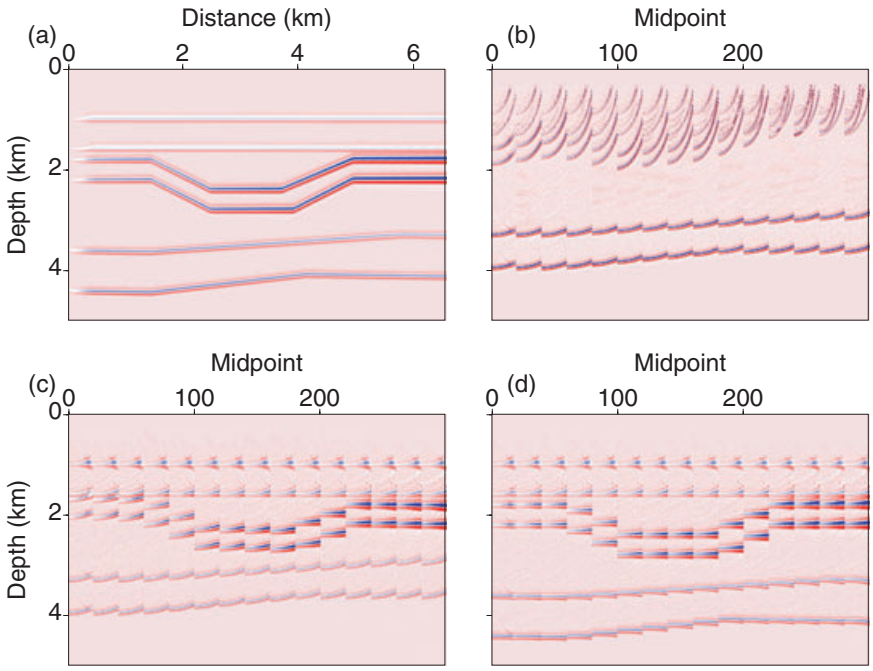

Figure 3 (a) Final image of the model from from Fig. 1 obtained after MVA and prestack depth migration for TTI media. The estimated parameters of the first (subsurface) layer are $k_z = 0.99\ s^{-1}$ and $k_x = \epsilon = \delta = 0$. For the second layer, $k_z = 0.59\ s^{-1}$, $k_x = 0.09\ s^{-1}$, $\epsilon = 0.09$ and $\delta = -0.11$. For the third layer, $k_z = 0.29\ s^{-1}$ and $k_x = \epsilon = \delta = 0$. The error for each parameter varies from ± 0.01 to ± 0.02, if the depth picking error is assumed to be ± 5 m. The other plots show image gathers obtained (b) with the initial model parameters before MVA; (c) after applying MVA to the two reflectors in the first (subsurface) layer; (d) after MVA for all three layers.

model because we estimate the velocity gradients by using image gathers at different depths and lateral positions. Here, however, we do not attempt to invert for the velocity V_{P0} at the top of the layer (it is specified *a priori*). To resolve ϵ, it is necessary to use nonhyperbolic moveout on long spreads, which is controlled by the anellipticity parameter $\eta \approx \epsilon - \delta$. Evidently, the relatively large offset-to-depth ratios (up to two) used in MVA are sufficient to provide a tight constraint on ϵ. The influence of spreadlength on the stability of parameter estimation is analysed in more detail below.

We also computed the error bars for each parameter by setting the standard deviation in the picked migrated depths on selected image gathers to ± 5 m. The picking errors are then substituted in the inversion operator to find the corresponding standard deviations of the model parameters (Sarkar and Tsvankin 2004). This procedure yields relatively small errors of up to ± 0.02 in the estimated anisotropy parameters.

The improvements achieved by the MVA algorithm in reducing the residual moveout in image gathers are illustrated in Figs 3(b) and 3(d). After applying MVA to the first two reflectors, image gathers of events in the first layer are flattened but there is substantial residual moveout in the two deeper layers (Fig. 3c). Upon completion of the parameter estimation for all three layers (that takes a total of 14 iterations), image gathers are flat throughout the model (Fig. 3d).

Sensitivity to spreadlength

To quantify the dependence of errors in the medium parameters on the maximum offset-to-depth ratio, we repeated MVA for the TTI syncline model with a range of spreadlengths. As before, the standard deviations were computed for a ± 5 m picking error in migrated depths. The increase in the offset-to-depth ratio (we used the depth of the midpoint of the dipping reflectors) makes estimation of all parameters more stable (Fig. 4). The parameters k_z, k_x and δ are constrained by NMO velocity, which can be measured on conventional-length spreads close to the reflector depth. For that reason, the error curves for k_z, k_x and δ show a similar trend and flatten out for offset-to-depth ratios between unity and 1.5.

In contrast, the error in the parameter ϵ continues to decrease until the maximum offset reaches twice the reflector depth. Indeed, ϵ in our model is constrained by the quartic moveout coefficient (i.e., by nonhyperbolic moveout), which is poorly resolved if the maximum offset-to-depth ratio is smaller than two (Tsvankin 2005). Thus, for stable estimation

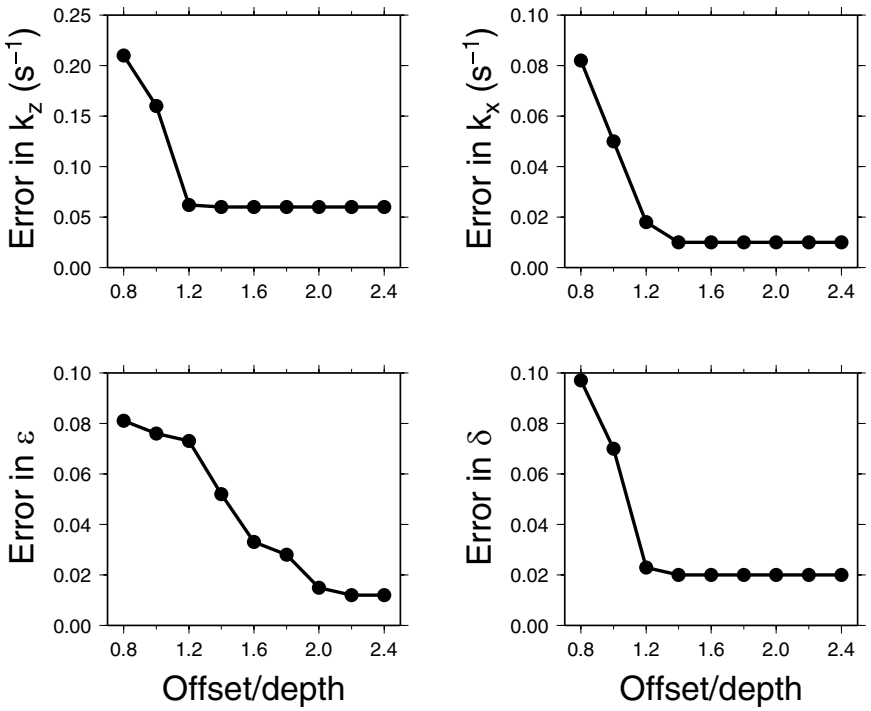

Figure 4 Influence of the maximum offset-to-depth ratio on the absolute errors in the parameters k_z, k_x, ϵ and δ. The errors are estimated from the MVA results for the left part of the syncline model in Fig. 1.

of all relevant parameters of TTI media it is highly desirable to employ offsets twice as large (or more) as the reflector depth.

Influence of noise

To assess the stability of our MVA and migration algorithms, we added random uncorrelated Gaussian noise to the synthetic data set for the model from Fig. 1. The signal-to-noise ratio (S/N), measured as the ratio of the peak signal amplitude to the root-mean-square (rms) amplitude of the background noise, is close to two; the frequency bands of the signal and noise are identical (Fig. 5a). The semblance maxima for most events in the presence of noise become less focused (Fig. 5b), which enhances the tradeoff between the moveout parameters r_1 and r_2 in equation (4) (Tsvankin 2005). However, since any pair of values (r_1, r_2) within the innermost semblance contour provides nearly the same variance of migrated depths, this tradeoff does not hamper the convergence of the MVA algorithm.

On the whole, despite the low S/N ratio, random noise does not significantly distort the MVA results (only the error in ϵ is non-negligible). Although the imaged reflectors are not as well focused as those on the noise-free section, they are clearly visible and correctly positioned (Fig. 5c).

Errors of VTI-based processing

Since most anisotropic imaging algorithms used in industry are designed for vertical transverse isotropy, it is important to evaluate the influence of the tilted symmetry axis on the quality of the migrated image. The section in Fig. 6 is obtained by setting the tilt in the syncline to zero, which makes the second layer VTI. Although the velocity model includes the correct values of ϵ and δ, the imaged dipping reflectors in the TTI layer are strongly misfocused and slightly shifted vertically. The image gathers for these dipping interfaces exhibit significant residual moveout (Fig. 6b), which indicates that the velocity field is inaccurate.

To reproduce a complete VTI processing sequence applied to this model, we repeated migration velocity analysis but without allowance for a tilted symmetry axis (i.e., the MVA code treated the second layer as VTI). After several iterations of parameter updating, the image gathers are largely flattened and the image quality is only marginally inferior to that achieved for the true model (Fig. 7). The parameters k_z, ϵ and δ of the second layer, however, are distorted. These errors are introduced by the MVA algorithm, which has to flatten image gathers in the TTI layer with the incorrect tilt of the symmetry axis. It is interesting to note that despite the

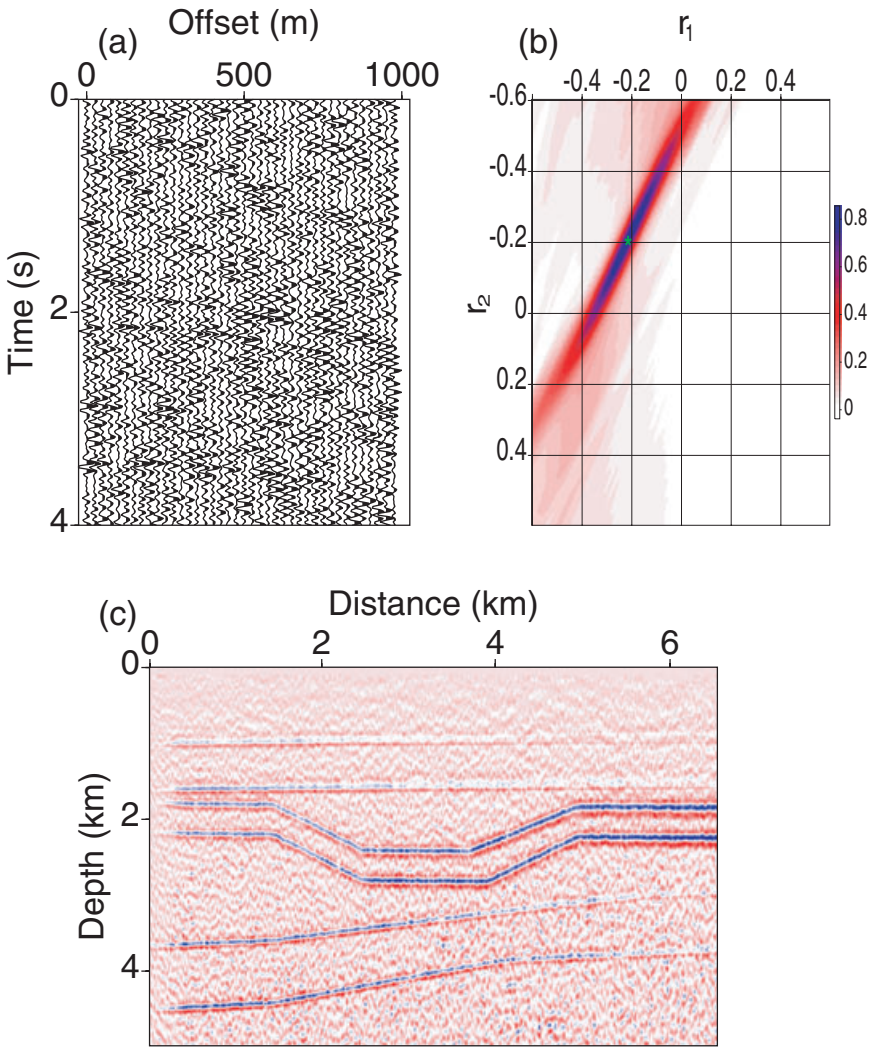

Figure 5 Influence of Gaussian noise on MVA and migration for the model from Fig. 1. (a) One of the noise-contaminated shot gathers (the lateral coordinate is close to 2 km). (b) The semblance scan for the bottom of the TTI layer (the lateral coordinate is 1.9 km) computed as a function of the moveout coefficients r_1 and r_2 (equation (4)). The maximum semblance is marked by the star. (c) The image obtained for the noise-contaminated data set. The estimated parameters of the first layer are $k_z = 1.06\ s^{-1}$, $k_x = 0.01\ s^{-1}$, $\epsilon = -0.01$ and $\delta = 0$. For the second layer, $k_z = 0.56\ s^{-1}$, $k_x = 0.11\ s^{-1}$, $\epsilon = 0.14$ and $\delta = -0.08$. For the third layer, $k_z = 0.35\ s^{-1}$, $k_x = 0.01\ s^{-1}$, $\epsilon = 0.02$ and $\delta = -0.02$. The errors for each parameter vary from ± 0.03 to ± 0.05 under the assumption that the picking error for the noisy data is ± 20 m.

distortions in ϵ and δ, the best-fit VTI model has an accurate value of the anellipticity parameter η.

The ability of the VTI-based algorithm to compensate for the influence of tilt decreases for larger relative thickness of the TTI syncline (Fig. 8). Because of the more significant contribution of the interval traveltime in the TTI layer, the dipping reflectors in Fig. 8 are misfocused and shifted in depth. Such artefacts generated by VTI imaging can serve as an indication that the medium immediately above the distorted reflectors may have a tilted symmetry axis. The quality of the image produced by VTI processing also decreases for strongly anisotropic TTI models with larger magnitudes of the parameters ϵ, δ and η.

Salt-dome model

The next test is performed for a simplified salt model, which can be considered typical for subsalt exploration plays. The section includes an isotropic salt dome with steep flanks overlaid by a TI shale formation. The symmetry axis in the shale is vertical directly above the dome and tilted (orthogonal to the bedding) in the dipping layers on both sides of the salt body

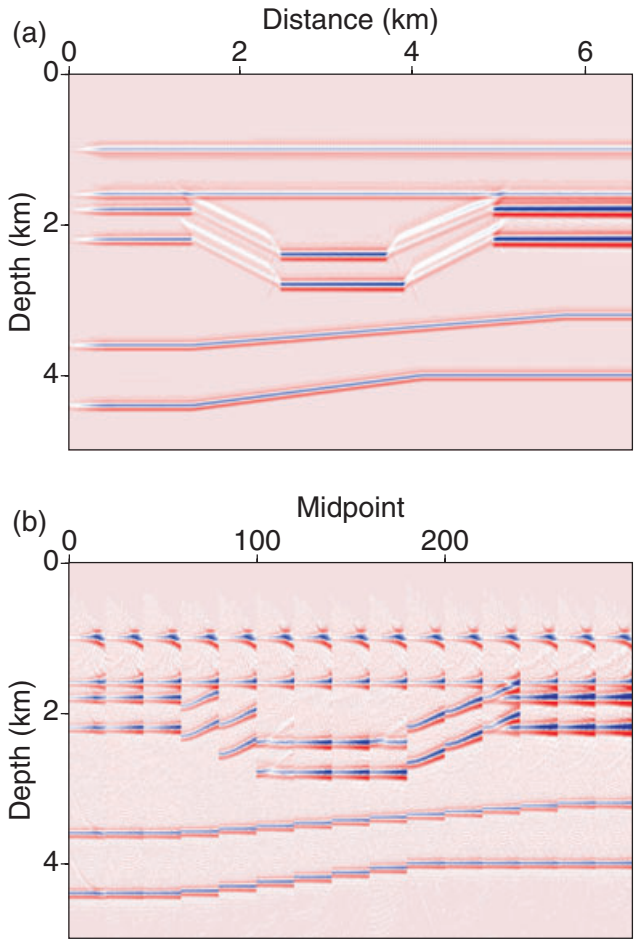

Figure 6 (a) Image of the model from Fig. 1 obtained without taking the symmetry-axis tilt in the second layer into account (i.e., the second layer is assumed to be VTI); the rest of the model parameters are correct. (b) The corresponding image gathers.

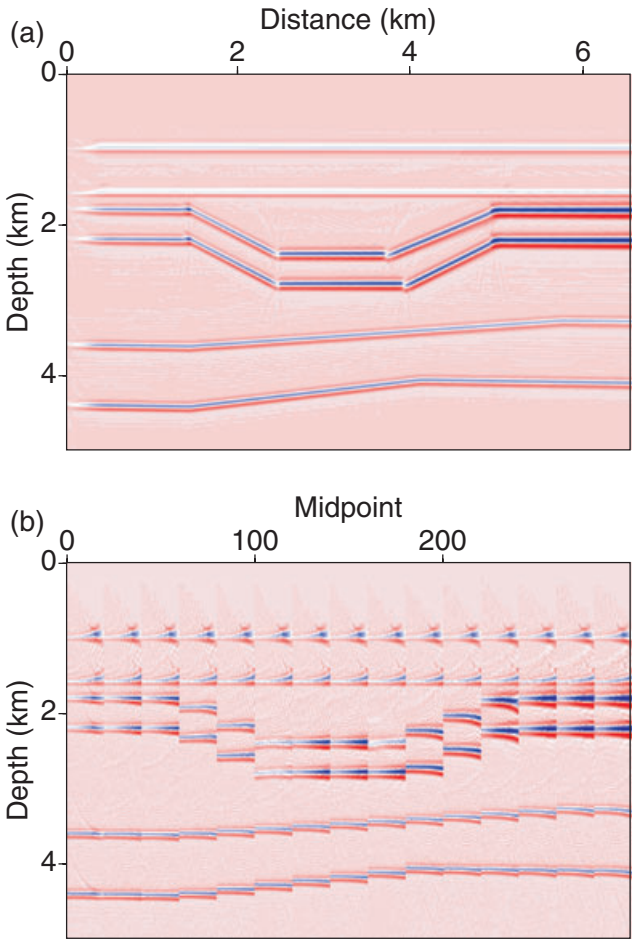

Figure 7 (a) Image of the model from Fig. 1 obtained after applying MVA under the assumption that the second layer is VTI. The estimated parameters of the second layer used in the migration are $k_z = 0.53\ s^{-1}$, $k_x = 0.12\ s^{-1}$, $\epsilon = 0.15$ and $\delta = -0.06$ ($\eta = 0.24$). (b) The corresponding image gathers.

(Fig. 9). TTI migration with the correct medium parameters produces a sharp, accurate image (Fig. 10a) and image gathers are flat even at the steep flanks of the salt (Fig. 10b).

Processing using TTI and VTI models

When tilt is properly taken into account by the MVA algorithm, both the dipping reflectors and the salt dome are well focused and properly positioned (Fig. 11). As before, the parameters are estimated in the layer-stripping mode using the correct values of the velocity V_{P0} at the top of each layer. For purposes of MVA, the shale formation was divided into two blocks along the vertical axis of the salt dome. Errors in the anisotropy parameters and velocity gradients are relatively small, although ϵ is not as well constrained as δ. The larger error in ϵ is expected because, as discussed above, this parameter does not influence NMO velocity and is obtained from nonhyperbolic moveout on long spreads.

Figure 12 shows the processing results for a velocity model that does not include tilt and treats the shale as VTI (the parameters ϵ, δ, k_z and k_x are correct). The substantial residual moveout in the image gathers for the dipping reflectors and pronounced image distortions indicate that the influence of tilt for this model is more significant than that for the TTI syncline model in Fig. 1.

Similar to the previous example, the VTI imaging result can be improved by deriving the best-fit VTI model from migration velocity analysis (Fig. 13). Although the reflectors inside and below the shale formation are better focused than those

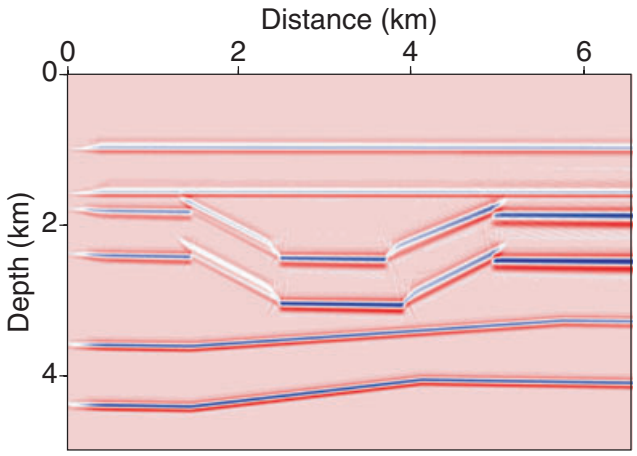

Figure 8 Same as Fig. 7(a) (i.e., the image obtained for the best-fit VTI model), but the thickness of the TTI layer from Fig. 1 is increased by 200 m. The estimated parameters are $k_z = 0.52\ s^{-1}$, $k_x = 0.12\ s^{-1}$, $\epsilon = 0.13$ and $\delta = -0.08$ ($\eta = 0.26$).

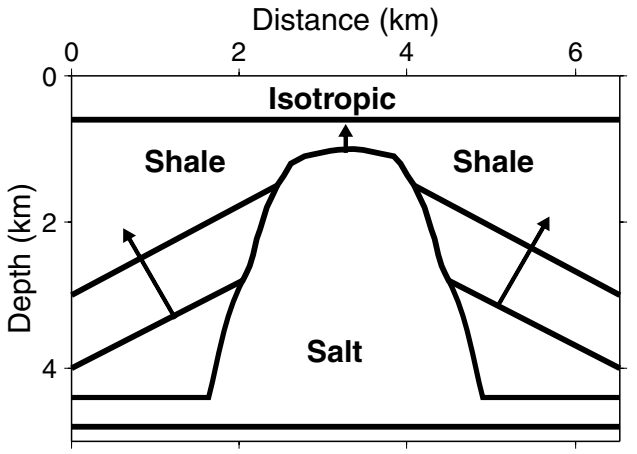

Figure 9 Simplified salt model that includes a salt dome overlaid by a TI shale formation. The symmetry axis in the shale (marked by the arrows) is vertical on top of the salt and orthogonal to the bedding in the uptilted layers, which are dipping at 30°. The parameters of the shale are $V_{P0} = 2.6$ km/s, $k_z = 0.6\ s^{-1}$, $k_x = 0.2\ s^{-1}$, $\epsilon = 0.3$ and $\delta = 0.15$. The subsurface horizontal layer is isotropic, with $V_{P0} = 1.5$ km/s, $k_z = 1.0\ s^{-1}$ and $k_x = \epsilon = \delta = 0$; for the salt dome and the blocks beneath the shale on both sides of the dome, $V_{P0} = 4.5$ km/s, $k_z = k_x = 0.1\ s^{-1}$ and $\epsilon = \delta = 0$.

in Fig. 12, the flanks of the salt body look blurry and are somewhat shifted laterally (Fig. 13a). Also, the image gathers exhibit significant residual moveout, especially near the salt (Fig. 13b). Evidently, the VTI model, which is obtained by flattening image gathers for the bottom of the shale layer dipping at 30°, is inadequate for the much steeper flanks of the salt dome.

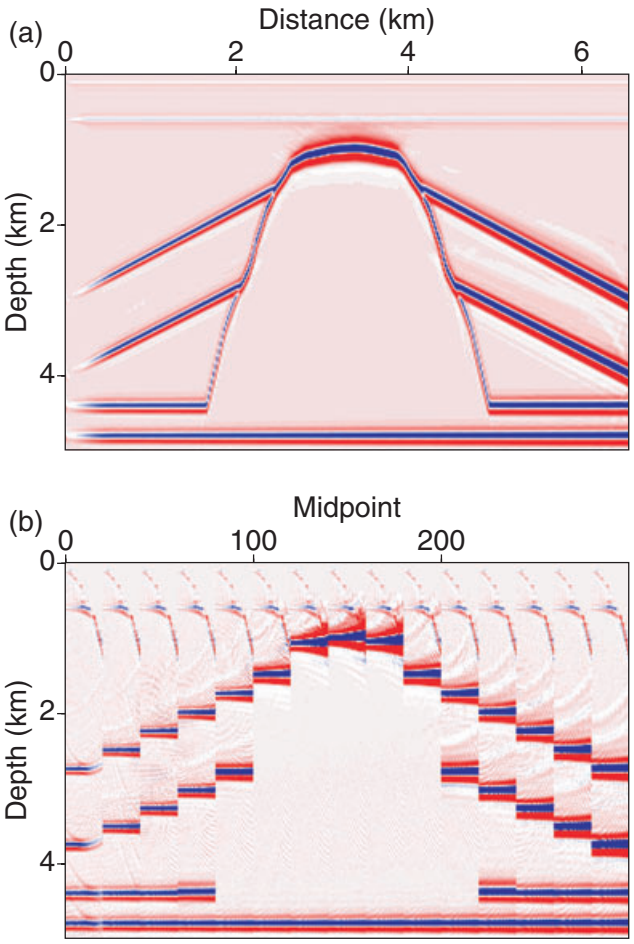

Figure 10 (a) True image of the model from Fig. 9 obtained by anisotropic prestack dept-migration with the correct parameters. (b) The corresponding image gathers.

Note that the improved image of the dipping reflectors in Fig. 13(a) is achieved by distorting the parameter δ and, to a lesser extent, the velocity gradients in the shale. Clearly, ignoring the tilt of the symmetry axis in dipping TI layers in the overburden may cause serious problems in imaging salt bodies (mostly in terms of focusing) and, therefore, subsalt reservoirs.

Thrust-sheet model

Complex tectonic processes in fold-and-thrust belts, such as the Canadian Rocky Mountain Foothills, sometimes produce bending shale layers with variable dip. Here, we process synthetic data generated for a TTI thrust sheet (Fig. 14) fashioned after the physical model of Leslie and Lawton (1996). This physical-modelling data set was used by Grechka *et al.*

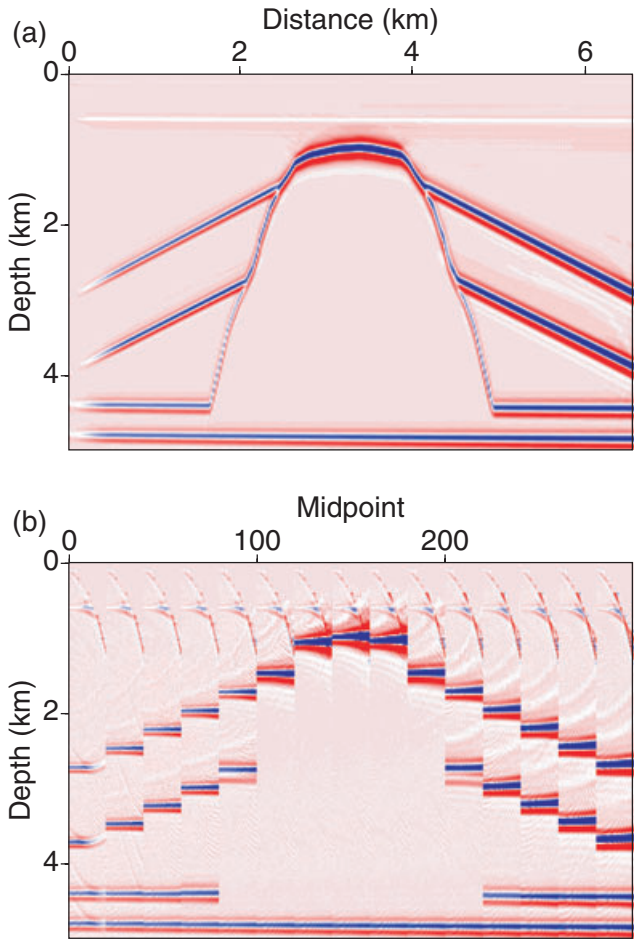

Figure 11 (a) Final image of the salt model obtained after MVA and prestack depth migration for TTI media. The estimated parameters of the first subsurface layer are $k_z = 0.97\ s^{-1}$ and $k_x = \epsilon = \delta = 0$. For the shale layer to the left of the salt, $k_z = 0.58\ s^{-1}$, $k_x = 0.19\ s^{-1}$, $\epsilon = 0.34$ and $\delta = 0.14$. To the right of the salt, $k_z = 0.59\ s^{-1}$, $k_x = 0.18\ s^{-1}$, $\epsilon = 0.32$ and $\delta = 0.15$. For the salt, $k_z = 0.09\ s^{-1}$, $k_x = 0.1\ s^{-1}$ and $\epsilon = \delta = 0$. The errors for each parameter vary from ± 0.01 to ± 0.03, if the depth picking error is assumed to be ± 5 m. (b) The corresponding image gathers.

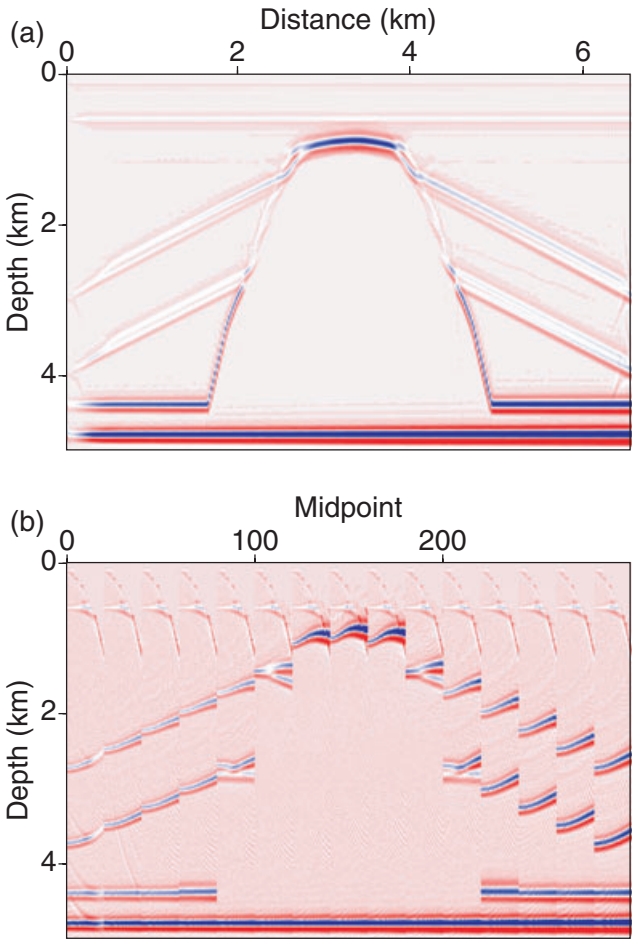

Figure 12 (a) Image of the model from Fig. 9 obtained without taking the symmetry-axis tilt into account; the rest of the model parameters are correct. (b) The corresponding image gathers.

(2001) for anisotropic parameter estimation. The algorithm of Grechka *et al.* (2001), however, operates only with NMO velocities measured on conventional spreads and relies on several simplifying assumptions about the model.

The benchmark image computed for the true model is shown in Fig. 15(a). Apart from relatively low amplitudes of steeply dipping events due to insufficient aperture, the reflectors are well focused and positioned and there is almost no residual moveout in Fig. 15(b). To apply the MVA algorithm, we divided the thrust sheet into four blocks that have distinctly different dips and carried out the parameter estimation separately for each block. As was the case for the previous two models, the TTI algorithm yields not only accurate parameter values but also a high-quality image (Fig. 16). Note that if the medium parameters (except for the tilt) are assumed to be the same in the blocks with different dips, there is no need to specify the symmetry-direction velocity V_{P0} in the TTI sheet.

When MVA does not take tilt into account, all boundaries in the thrust sheet are poorly focused, with noticeable artefacts at the points where the interfaces change dip (Fig. 17a). It is interesting that the errors in the medium parameters produced by the VTI velocity analysis are relatively minor. Apparently, image gathers for the thrust sheet (Fig. 17b) could not be flattened by distorting the anisotropy parameters or velocity gradients, if the symmetry axis is vertical. As was the case for the salt-dome model, the VTI algorithm cannot handle reflectors (here, the boundaries of each block) with substantially

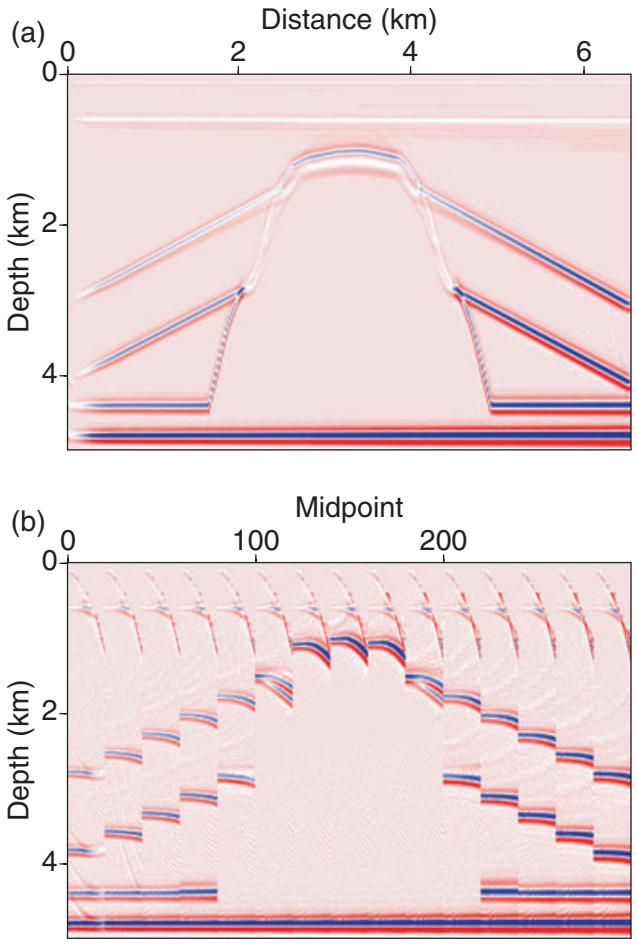

Figure 13 (a) Image of the model from Fig. 9 obtained after applying MVA under the assumption that the shale formation is VTI. The estimated parameters for the shale layer to the left of the salt are $k_z = 0.62\ s^{-1}$, $k_x = 0.17\ s^{-1}$, $\epsilon = 0.32$ and $\delta = 0.12$. To the right of the salt, $k_z = 0.62\ s^{-1}$, $k_x = 0.18\ s^{-1}$, $\epsilon = 0.30$ and $\delta = 0.11$. (b) The corresponding image gathers.

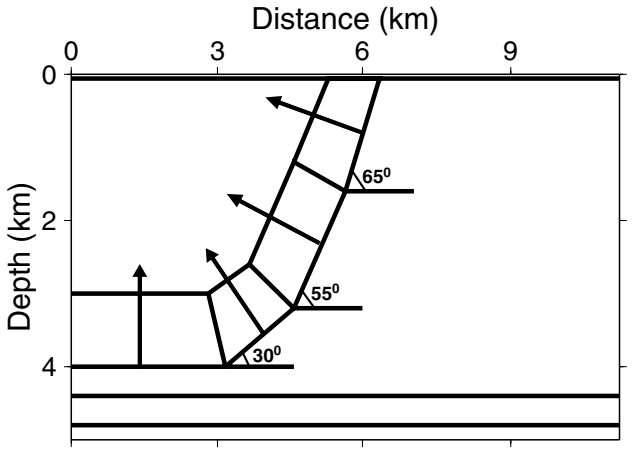

Figure 14 TTI thrust sheet with variable dip for different blocks (0°, 30°, 55° and 65°) and the symmetry axis (marked by the arrows) orthogonal to the sheet's bottom. Except for the symmetry-axis direction, the parameters of all TTI blocks are the same: $V_{P0} = 2.3$ km/s, $k_z = 0.6\ s^{-1}$, $k_x = 0.1\ s^{-1}$, $\epsilon = 0.1$ and $\delta = -0.1$. The rest of the model is composed of isotropic layers. The subsurface (weathering) layer is thin (60 m) and has $V_{P0} = 1.5$ km/s, $k_z = 1.0\ s^{-1}$, and $k_x = \epsilon = \delta = 0$; the velocity V_{P0} across the bottom of the layer is continuous. For the medium around the TTI sheet, $k_z = 1.0\ s^{-1}$ and $k_x = \epsilon = \delta = 0$. The horizontal layer at the bottom of the model has $V_{P0} = 3.5$ km/s, $k_z = 0.3\ s^{-1}$ and $k_x = \epsilon = \delta = 0$.

different dips. Also, the VTI model becomes inadequate for the most shallow segment of the thrust sheet, which has a large tilt of 65°.

DISCUSSION AND CONCLUSIONS

The combination of tilted transverse isotropy (TTI) and structural complexity in many important exploration plays makes it imperative to apply advanced migration velocity analysis (MVA) methods and prestack depth imaging. Here, we presented an MVA methodology for P-waves in heterogeneous TTI media based on dividing the model into "quasi-factorized" blocks. The anisotropy parameters ϵ and δ in each block are constant, while the symmetry-direction velocity V_{P0} represents a linear function of the spatial coordinates and is described by the vertical (k_z) and lateral (k_x) gradients. To reduce the uncertainty in parameter estimation, the symmetry axis in each block or layer is taken to be orthogonal to the reflector at the bottom of the block. Since reflectors may have arbitrary shape, the symmetry-axis orientation generally varies in space, which means that blocks are not fully factorized. (In factorized TI media, the symmetry-axis direction is fixed).

Our algorithm represents an extension to TTI media of the MVA methodology developed by Sarkar and Tsvankin (2004) for vertical transverse isotropy. MVA is combined with Kirchhoff prestack depth migration based on anisotropic ray tracing for heterogeneous TI media with arbitrary tilt. Parameter estimation is performed in the layer-stripping mode starting at the surface, with the symmetry-direction velocity V_{P0} either specified at a single point in each block or assumed to be continuous in the vertical direction. To estimate the vertical gradient k_z, we use image gathers for at least two reflectors at different depths within each block.

If the velocity V_{P0} is known, the parameter δ in TTI media with the symmetry axis orthogonal to the reflector can be

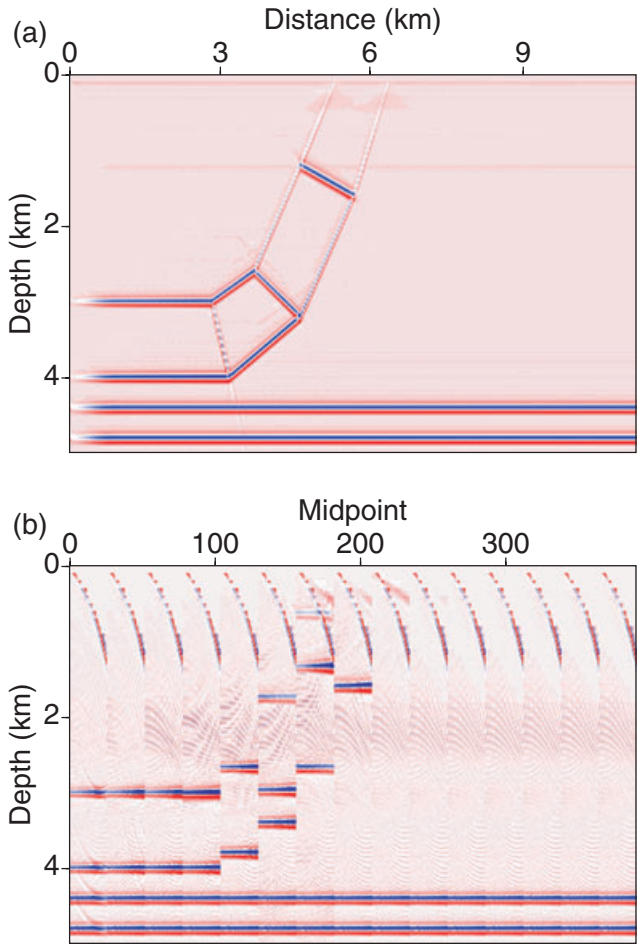

Figure 15 (a) True image of the model from Fig. 14 obtained by anisotropic prestack depth migration with the correct parameters. (b) The corresponding image gathers.

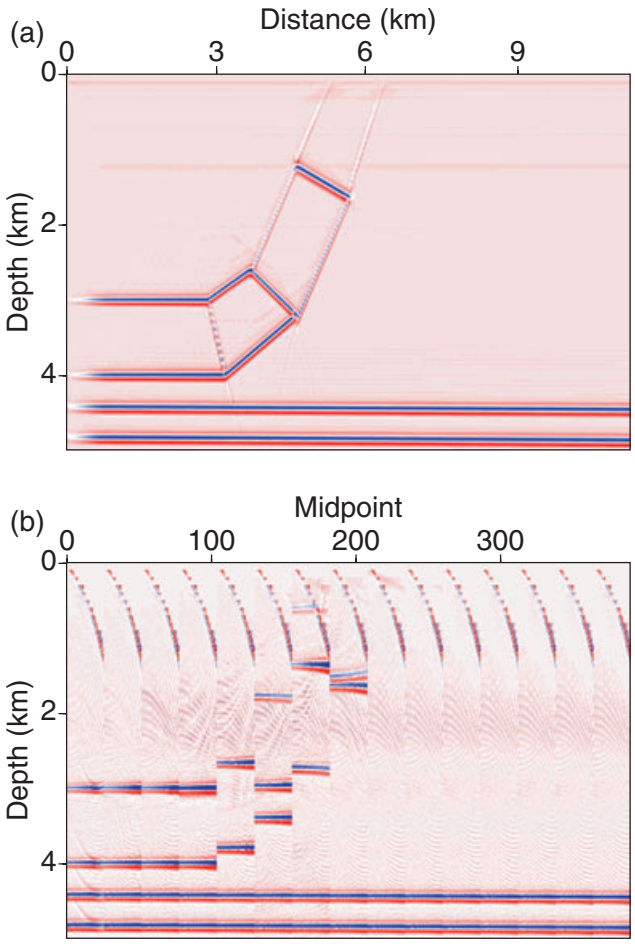

Figure 16 (a) Final image of the thrust model obtained after MVA and prestack depth migration for TTI media. The parameters were estimated for each block of the thrust sheet (i.e., for each dip) separately. For the horizontal TTI block (dip=0°), $k_z = 0.62\ s^{-1}$, $k_x = 0.11\ s^{-1}$, $\epsilon = 0.11$ and $\delta = -0.09$; for the 30° dip, $k_z = 0.59\ s^{-1}$, $k_x = 0.12\ s^{-1}$ $\epsilon = 0.09$ and $\delta = -0.11$; for the 55° dip, $k_z = 0.58\ s^{-1}$, $k_x = 0.09\ s^{-1}$ $\epsilon = 0.11$ and $\delta = -0.08$; for the 65° dip, $k_z = 0.62\ s^{-1}$, $k_x = 0.12\ s^{-1}$, $\epsilon = 0.09$ and $\delta = -0.1$. For the horizontal layer beneath the TTI sheet, $k_z = 0.29\ s^{-1}$, $k_x = \epsilon = 0$ and $\delta = 0.01$. The errors for each parameter vary from ± 0.01 to ± 0.03, if the depth picking error is assumed to be ± 5 m. (b) The corresponding image gathers.

constrained using the NMO velocities for either horizontal or dipping events. Estimation of the parameters η and ϵ in TTI media generally requires using nonhyperbolic moveout. In our MVA algorithm, the residual moveout in long-spread image gathers is evaluated using the two-parameter nonhyperbolic equation described by Sarkar and Tsvankin (2004). We find that sufficiently stable estimation of the parameter ϵ can be achieved if the offset-to-depth ratio reaches at least two.

The MVA and migration algorithms were tested on several typical TTI models including a syncline, a salt dome with dipping TTI layers on both sides and a bending TTI layer (thrust sheet). For all three models we were able to accurately reconstruct the velocity gradients k_z and k_x throughout the medium and the anisotropy parameters ϵ and δ in the TTI blocks. The migrated sections computed with the estimated velocity model are practically indistinguishable from the true images, with good focusing and positioning of reflectors beneath the TTI formations. The number of iterations of velocity analysis needed to flatten image gathers for our synthetic models does not exceed 20 but it may be larger for a more complicated subsurface structure.

To assess the influence of tilt on image quality, we migrated the data with the VTI model (i.e., with zero tilt) that has the correct values of V_{P0}, k_z, k_x, ϵ and δ. Although the tilt in

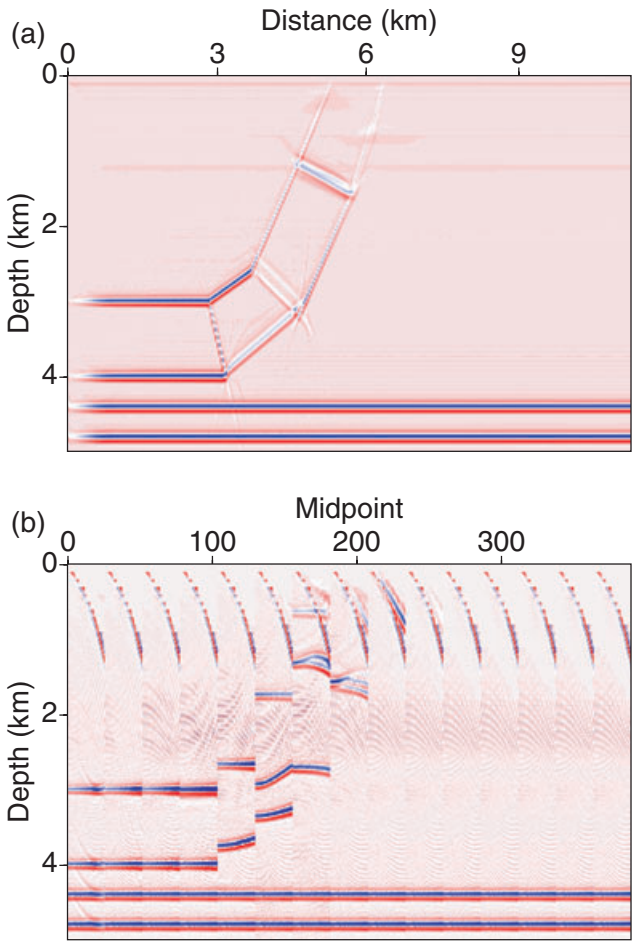

Figure 17 (a) Image of the model from Fig. 14 obtained after applying MVA under the assumption that the thrust sheet is VTI. The parameters of the horizontal block (dip=0°) are $k_z = 0.59\ s^{-1}$, $k_x = 0.09\ s^{-1}$, $\epsilon = 0.09$ and $\delta = -0.11$; for the 30° dip, $k_z = 0.62\ s^{-1}$, $k_x = 0.11\ s^{-1}$, $\epsilon = 0.11$ and $\delta = -0.09$; for the 55° dip, $k_z = 0.61\ s^{-1}$, $k_x = 0.1\ s^{-1}$, $\epsilon = 0.13$ and $\delta = -0.12$; and for the 65° dip, $k_z = 0.63\ s^{-1}$, $k_x = 0.13\ s^{-1}$, $\epsilon = 0.11$ and $\delta = -0.08$. (b) The corresponding image gathers.

our first two models (the syncline and salt dome) is moderate (30°), setting it to zero results in significant degradation of image quality. The inaccuracy of the VTI velocity field also manifests itself through substantial residual moveout in image gathers.

In order to emulate a complete VTI processing sequence applied to TTI media, we performed MVA without allowance for a tilted symmetry axis to obtain the 'best-fit' VTI model. The MVA algorithm can achieve partial flattening of image gathers with the incorrect (zero) tilt but at the expense of distorting the medium parameters, especially ϵ and δ (although the value of η remains accurate). Such artificial adjustments in ϵ and δ improve image quality, although migrated sections typically are inferior to those generated with the TTI model. Also, the ability of the VTI-based algorithm to compensate for the influence of tilt decreases for more complicated models and TTI layers with relatively large thickness or strong anisotropy.

On the whole, the MVA methodology introduced here provides a practical tool for building TTI velocity models with some *a priori* information. Combined with prestack depth migration, this MVA algorithm can be efficiently used to image targets beneath TTI formations in structurally complex environments.

ACKNOWLEDGEMENTS

We are grateful to the A(nisotropy)-Team of the Center for Wave Phenomena (CWP), Colorado School of Mines (CSM) and other colleagues at CWP for fruitful discussions. Laxmidhar Behera thanks the Department of Science and Technology, Govt. of India, for awarding him the BOYSCAST Fellowship and V. P. Dimri, Director of the National Geophysical Research Institute, Council of Scientific and Industrial Research, for granting him permission to pursue postdoctoral research in CWP. The constructive suggestions of the editors and reviewers of *Geophysical Prospecting* helped to improve the paper. This work was partially supported by the Consortium Project on Seismic Inverse Methods for Complex Structures at CWP.

REFERENCES

Alkhalifah T. 1995. Efficient synthetic-seismogram generation in transversely isotropic, inhomogeneous media. *Geophysics* **60**, 1139–1150.

Alkhalifah T. and Tsvankin I. 1995. Velocity analysis for transversely isotropic media. *Geophysics* **60**, 1550–1566.

Angerer E., Horne S.A., Gaiser J.E., Walters R., Bagala S. and Vetri L. 2002. Characterization of dipping fractures using PS mode-converted data. 72nd SEG meeting, Salt Lake City, Utah, USA, Expanded Abstracts, 1010–1013.

Červený V. 1989. Ray tracing in factorized anisotropic inhomogeneous media. *Geophysical Journal International* **99**, 91–100.

Dewangan P. and Tsvankin I. 2006a. Modeling and inversion of PS-wave moveout asymmetry for tilted TI media: Part 1 – Horizontal TTI layer. *Geophysics* **71**, D107–D121.

Dewangan P. and Tsvankin I. 2006b. Modeling and inversion of PS-wave moveout asymmetry for tilted TI media: Part 2 – Dipping TTI layer. *Geophysics* **71**, D123–D134.

Grechka V. and Tsvankin I. 2000. Inversion of azimuthally dependent NMO velocity in transversely isotropic media with a tilted axis of symmetry. *Geophysics* **65**, 232–246.

Grechka V., Pech A., Tsvankin I. and Han B. 2001. Velocity analysis for tilted transversely isotropic media: A physical modeling example. *Geophysics* **66**, 904–910.

Isaac J.H. and Lawton D.C. 1999. Image mispositioning due to dipping TI media: A physical modeling study. *Geophysics* **64**, 1230–1238.

Kumar D., Sen M.K. and Ferguson R.J. 2004. Traveltime calculation and prestack depth migration in tilted transversely isotropic media. *Geophysics* **69**, 37–44.

Leslie J.M. and Lawton D.C. 1996. Structural imaging below dipping anisotropic layers: Predictions from seismic modeling. 66th SEG meeting, Denver, Colorado, USA, Expanded Abstracts, 719–722.

Liu Z. and Bleistein N. 1995. Migration velocity analysis: Theory and an iterative algorithm. *Geophysics* **60**, 142–153.

Pech A., Tsvankin I. and Grechka V. 2003. Quartic moveout coefficient: 3D description and application to tilted TI media. *Geophysics* **68**, 1600–1610.

Sarkar D. and Tsvankin I. 2003. Analysis of image gathers in factorized VTI media. *Geophysics* **68**, 2016–2025.

Sarkar D. and Tsvankin I. 2004. Migration velocity analysis in factorized VTI media. *Geophysics* **69**, 708–718.

Sarkar D. and Tsvankin I. 2006. Anisotropic migration velocity analysis: Application to a data set from West Africa. *Geophysical Prospecting* **54**, 575–587.

Thomsen L. 1986. Weak elastic anisotropy. *Geophysics* **51**, 1954–1966.

Tsvankin I. 1995. Normal moveout from dipping reflectors in anisotropic media. *Geophysics* **60**, 268–284.

Tsvankin I. 1997. Moveout analysis for transversely isotropic media with a tilted symmetry axis. *Geophysical Prospecting* **45**, 479–512.

Tsvankin I. 2005. *Seismic Signatures and Analysis of Reflection Data in Anisotropic Media,* 2nd edn. Elsevier.

Vestrum R., Lawton D.C. and Schmid R. 1999. Imaging structures below dipping TI media. *Geophysics* **64**, 1239–1246.